EDISON 16 IOP Publishing
Journal of Physics: Conference Series **193** (2009) 012103 doi:10.1088/1742-6596/193/1/012103

Prediction of giant intrinsic spin-Hall effect in strained p-GaAs quantum wells

C Schindler and P Vogl

Walter Schottky Institut, Technische Universitaet Muenchen, Am Coulombwall 3, 85748 Garching, Germany

E-mail: Christoph.Schindler@wsi.tum.de

Abstract. We perform spin resolved non-equilibrium Green's function calculations in nanostructured, strained two-dimensional GaAs electron and hole gases. Inelastic scattering is taken into account. We show theoretically that the intrinsic inverse spin-Hall effect provides a simple, sensitive, and purely electrical scheme to measure the spin polarization in nanostructures. We predict large spin polarizations and spin-Hall voltages for several concrete device geometries. We propose tensile strained p-GaAs as being optimally suited for detecting the inverse spin Hall effect and show that the effect is absent in n-GaAs.

1. Introduction

The intrinsic spin-Hall effect (SHE) in semiconductors predicted by Murakami *et al.* [1] and Sinova *et al.* [2] is a very promising candidate to manipulate the spin degree of freedom without ferromagnetic elements or external magnetic fields and to generate spin polarized currents, solely caused by the spin-orbit interaction (SOI). The intrinsic SHE has been detected experimentally in semiconductors for two dimensional (2D) hole gases by optical means [3]. However, there are no published reports yet on purely transport based measurements of spin currents in semiconductors, in contrast to metallic systems [4]. In particular, the intrinsic inverse spin-Hall effect that converts a spin polarization into an electric bias, has not yet been observed in semiconductors. In this paper, we predict concrete nanostructured materials and device geometries that exhibit a large intrinsic inverse spin-Hall effect. We provide detailed studies of an H-shaped 2DHG originally proposed by Hankiewicz *et al.* [5] and for several more complex three terminal devices.

2. Model and theoretical approach

The investigated 2D geometries are shown schematically in figure 1. For the structure shown in figure 1(a), an applied source-drain bias drives a charge current in the lower leg. Due to the spin-Hall effect, a spin current flows through the vertical connection into the upper leg that, in turn, induces a voltage drop between the two gates due to the inverse spin-Hall effect [5]. For the second, T-shaped, geometry a voltage is applied between the top source contact and the two bottom drain contacts to the right and to the left of the horizontal arm. We have shown previously [6] that large spin polarizations are generated close to the two drain contacts in figure 1(b) that causes the current in the horizontal bar to be spin polarized. To convert this polarization into an electrical bias voltage, we add two analyzing vertical bars into the right and left horizontal arms figure 1(c). The vertical gates exhibit a finite voltage drop in proportion to the spin-polarized current flowing towards the drain contacts. The principle is closely related to the anomalous Hall effect and has been used experimentally in metallic

© 2009 IOP Publishing Ltd

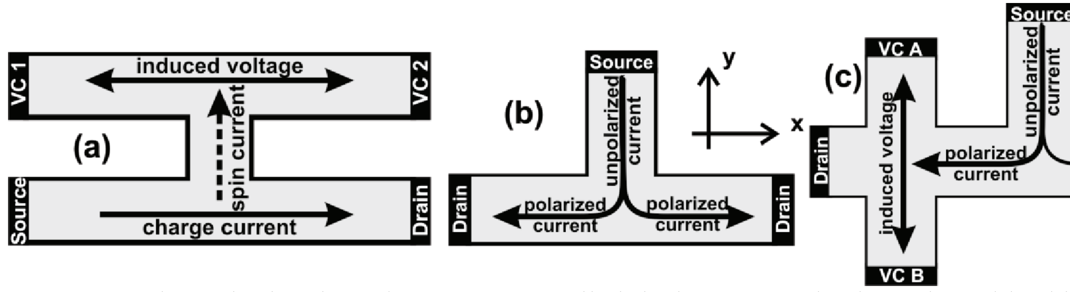

Figure 1. Schematic drawing of top gate controlled device geometries investigated in this paper. (a) H-shaped structure, (b) T-shaped structure, and (c) extended T-shaped structure.

systems, where the polarized current has been injected from a ferromagnet [7]. In our case, the spin polarized current is generated directly by the T-shaped geometry due to the intrinsic SHE.

We model the 2D system by a single-band effective mass Hamiltonian including the SO interaction up to cubic order in the in-plane momentum **k**. For a quantum well with D_{2d} symmetry we have [8]

$$H = \frac{\hbar^2 k^2}{2m^*} + V(x,y) + \alpha\big(k_x\sigma_x - k_y\sigma_y\big) + c_1\big(k_y\sigma_x - k_x\sigma_y\big)k_x k_y + c_2(k_x^3\sigma_x - k_y^3\sigma_y), \tag{1}$$

where $V(x,y)$ is the confinement potential and σ_i $(i = x,y,z)$ are the Pauli matrices. The last three terms in equation (1) arise from the SOI and correspond to an effective magnetic field often called the spin-orbit field. The k-linear term proportional to α is the Dresselhaus coupling [9]. There is no Rashba coupling since we only deal with D_{2d} symmetric structures in this paper. The coupling constants α, c_1, and c_2 as well as the effective mass m^* are obtained from atomistic tight binding calculations based on a relativistic $sp^3d^5s^*$ parameterization [10]. For a given band, we map the full atomistic tight-binding matrix onto the 2×2 effective mass Hamiltonian equation (1). We thereby include the effects of all other bands non-perturbatively.

We employ the non-equilibrium Green's function (NEGF) method for open systems [11], generalized to spin systems [12]. For stationary transport, the two spin resolved Green's functions, the retarded Green function $G^R_{\sigma,\sigma'}(\mathbf{r},\mathbf{r}')$ and the lesser Green function $G^<_{\sigma,\sigma'}(\mathbf{r},\mathbf{r}')$ namely, fully describe the system. Here, σ, σ' are spin indices. We include scattering by energy, momentum and spin relaxing Büttiker probes [13]. These probes have been modeled in such a way as to mimic realistic mobilities in 2D electron and hole gases. For the hole gases investigated in this paper, we assume a phase breaking mean free path of 200 nm. In this way, known artifacts of purely ballistic transport are eliminated [14]. In the numerical implementation, we solve the NEGF equations in real space by employing a finite difference scheme. Importantly, we apply open boundary conditions, i.e. the device gets attached to two or more semi-infinite leads which remain in thermal equilibrium. In addition, they include the same spin-orbit terms as the active device to suppress artificial reflections that are caused by the abrupt device-lead interfaces.

3. Results and discussion

The present atomistic electronic calculations show an exceptionally large k-linear SOI for the top valence band in tensile strained GaAs quantum wells [15]. This large k-linear spin splitting is caused by the strain, which may be generated by growing GaAs on $In_xAl_{1-x}As$ buffer material. Figure 2 shows the calculated Dresselhaus coupling constant within a 14 nm GaAs quantum well as a function of the strain that is generated by embedding the GaAs layer within $In_xAl_{1-x}As$ that sets the lateral lattice constant and acts as barrier material. We note that the SOI in the conduction band remains unaffected by the strain. The tensile strain causes the light hole band to lie above and to be well separated from the heavy hole band. For the other parameters we obtain only a weak dependence on x. We find $m^* \approx .375$, $c_1 \approx -65$ meVnm^3, and $c_2 \approx 15$ meVnm^3.

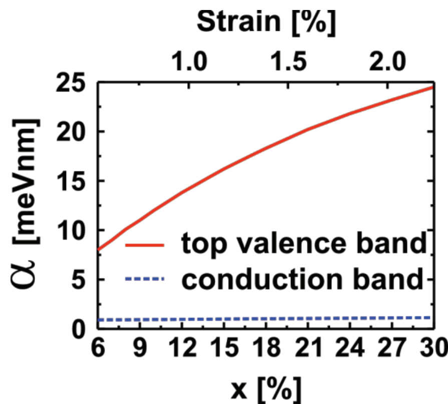

Figure 2. Calculated k-linear Dresselhaus coupling constant α in meVnm for a 14 nm wide strained GaAs quantum well plotted versus the Indium content x in % (bottom axis) and tensile strain in % (top axis). The red line (solid) is for the top valance band, while the blue one (dashed) is for the conduction band.

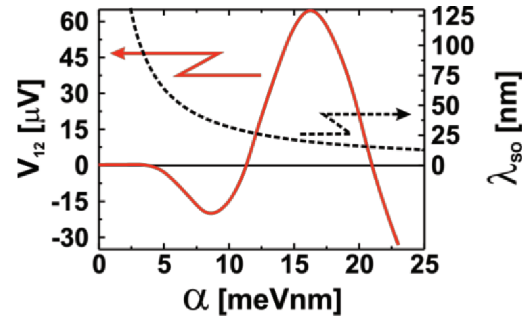

Figure 3. Calculated spin-Hall voltage V_{12} in μV and the spin precession length λ_{SO} in nm as a function of the Dresselhaus coupling constant α in meVnm. The charge density n_{2D} = 1.75×10^{11}cm^{-2} and the applied bias V_{SD} = .5 mV are kept fixed.

We now turn to the device with H-bar geometry as shown in figure 1(a) and consider a hole gas in a tensile strained GaAs quantum well. We assume the widths of all channels to be equal to 30 nm. The length of the vertical bar is also taken to be 30 nm. In figure 3, we show the calculated spin-Hall voltage V_{12} between voltage contact (VC) 1 and 2 (cf. figure 1(a)) as a function of the SOI strength for an applied source-drain bias V_{SD} =.5 mV. The hole density amounts to ~1.75×1011 cm^{-2} so that only the highest hole subband is occupied. The calculations show an oscillatory behavior of the spin-Hall voltage V_{12} as a function of the SOI strength which can be explained as follows. The magnitude and sign of the spin-Hall voltage V_{12} is roughly proportional to the average out-of-plane spin polarization $\langle P_z \rangle$ in the hole gas in the upper leg that has been induced by the charge current in the lower leg. With increasing SOI, the spin precession length λ_{SO} changes as depicted in figure 3. Whenever the device width is an even (odd) integer of this length, $\langle P_z \rangle$ becomes a maximum or minimum (zero) which explains the finding in figure 3. For $\alpha < 5$ meVnm, the calculated spin-Hall voltage is negligible. Therefore, the intrinsic inverse SHE is negligible in n-type GaAs, which holds independently of the mobility. For the strained p-GaAs wells, by contrast, the two extrema in figure 3 correspond to a fairly low Indium composition of x=7% and x=15%. The resistance signal, i.e. the spin-Hall voltage V_{12} divided by the source-drain current I_{SD}, is approximately 1 kΩ for x=7% and 3 kΩ for x=15%, which is markedly larger than those predicted for HgTe quantum wells [16]. Figure 4 shows the spin-Hall voltage V_{12} and the source-drain current I_{SD} as a function of applied source-drain bias V_{SD} for both structures. Since the current is almost equal in both cases, in contrast to the spin-Hall voltage V_{12}, we can be sure that the latter is caused by the SOI rather than by a change in the longitudinal conductance.

For the T-shaped device in figure 1(b), we use the same channel widths and hole density as for the H-shaped geometry. Figure 5 shows the three components of the spin polarization at the rightmost drain contact as a function of the length of the side arm. The y- and z-component of the spin polarization, averaged over the width of the arm, is predicted to oscillate in correspondence with the spin precession length. The x-component lies parallel to the spin-orbit field and therefore does not precess. All polarization amplitudes decrease in magnitude due to the phase breaking scattering.

Finally, we attach additional analyzing probes (VC A and VC B) to the T-structure as depicted in figure 1(c). The calculated spin-Hall voltage V_{AB} turns out to be a direct measure for the z-component of the spin polarization. When the probe is attached at a position where positively (negatively)

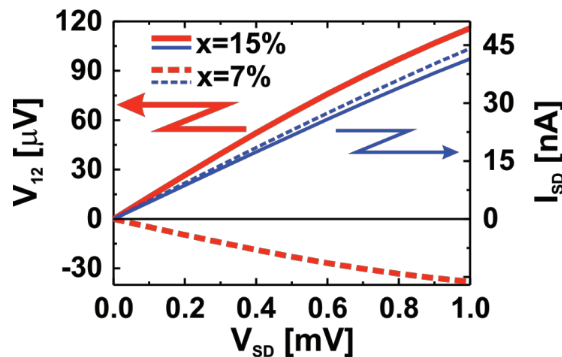

Figure 4. Calculated spin-Hall voltage V_{12} (left vertical axis, thick red lines) and the source-drain current I_{SD} in nA (right vertical axis, thin blue lines), as a function of V_{SD}. Shown are results for two different strain values. The dashed lines are for an Indium content of x=7%, while the solid ones are for x=15%.

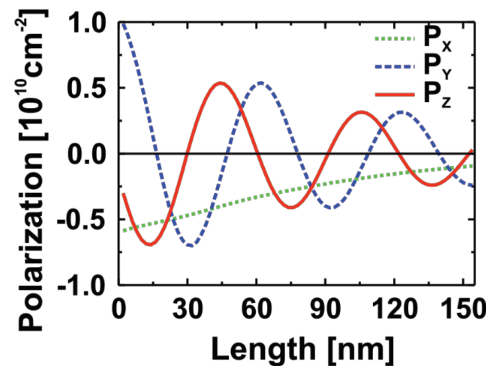

Figure 5. Calculated spin polarization averaged along the y-direction at the right drain contact in cm^{-2}, as a function of the length of the side arm in nm. Red (solid) shows the z-component, blue (dashed) the y-component, and green (dotted) the x-component. The Indium content is 9% and the applied bias equals 1.0 mV.

polarized carriers dominate, we obtain a positive (negative) voltage signal V_{AB}. If we attach the probe at 75 nm, for example, we find V_{AB} = -15.6 μV.

Acknowledgments

The authors acknowledge financial support from the Deutsche Forschungsgemeinschaft (SPP 1285), and the Nano Initiative Munich.

References

[1] Murakami S, Nagaosa N and Zhang S C 2003 *Science* **301** 1348
[2] Sinova J, Culcer D, Niu Q, Sinitsyn N A, Jungwirth T and MacDonald A H 2004 *Phys. Rev. Lett.* **92** 126603
[3] Wunderlich J, Kaestner B, Sinova J and Jungwirth T 2005 *Phys. Rev. Lett.* **94** 047204
[4] Saitoh E, Ueda M, Miyajima H and Tatara G 2006 *Appl. Phys. Lett*. **88** 182509
[5] Hankiewicz E M, Molenkamp L W, Jungwirth T and Sinova J 2004 *Phys. Rev.* B **70** 241301(R)
[6] Kubis T and Vogl P 2008 *phys. stat. sol*. (c) **5** 290
[7] Valenzuela S O and Tinkham M 2007 *J. Appl. Phys*. **101** 09B103
[8] von Allmen P 1992 *Phys. Rev.* B **46** 15382
[9] Fabian J, Matos-Abiague A, Ertler C, Stano P and Zutic I 2007 *acta physica slovaca* **4** 565
[10] Jancu JM, Scholz R, Beltram F and Bassani F 1998 *Phys. Rev.* B **57** 6493
[11] Datta S 1999 *Electronic Transport in Mesoscopic Systems* (Cambridge: Cambridge University Press)
[12] Nicolic B K, Zarbo L P and Souma S 2006 *Phys. Rev.* B **73** 075303
[13] Venugopal R, Paulsson M, Goasguen S, Datta S and Lundstrom M S 2003 *J. Appl. Phys*. **93** 5613
[14] Mamaluy D, Vasileska D, Sabathil M, Zibold T and Vogl P 2005 *Phys. Rev.* B **71** 245321
[15] Majewski J A and Vogl P 2003 *Physics of Semiconductors 2002* (Bristol: Institut of Physics Publ.) p 305
[16] Brune C, Roth A, Novik E G, Konig M, Buhmann H, Hankiewicz E M, Hanke W, Sinova J and Molenkamp L W 2008 (*Preprint* cond-mat/0812.3768v1)